

RESEARCH ARTICLE

In situ Mg isotope measurements of biogenic carbonates using laser ablation multi-collector inductively coupled plasma mass spectrometry: A new tool to understand biomineralisation

Aleksey Sadekov¹  | Nicholas S. Lloyd²  | Sambuddha Misra³ |
Juan Pablo D'Olive^{1,4} | Malcolm McCulloch¹

¹Ocean Graduate School, The ARC Centre of Excellence for Coral Reef Studies, The University of Western Australia, Perth, 6009, Australia

²Thermo Fisher Scientific, Hanna-Kunath-Str. 11, Bremen, 28119, Germany

³Centre for Earth Sciences, Indian Institute of Science, Bangalore, 560012, India

⁴Institute of Geological Sciences, Freie Universität Berlin, Berlin, 12249, Germany

Correspondence

A. Sadekov, Ocean Graduate School, The ARC Centre of Excellence for Coral Reef Studies, The University of Western Australia, Perth 6009 Australia.

Email: aleksey.sadekov@uwa.edu.au

Funding information

ERC Advanced Grant, Grant/Award Number: 2010 NEWLOG ADG-267931; ARC Laureate Fellowship, Grant/Award Number: FL120100049; ARC Centre of Excellence for Coral Reef Studies, Grant/Award Number: CE140100020

Rationale: Magnesium is one of the most abundant elements in the earth's crust and in seawater. Fractionation of its stable isotopes has been shown to be a useful indicator of many geological, chemical, and biological processes. For example, biogenic carbonates display an ~5‰ range of $\delta^{26}\text{Mg}$ values, which is attributed to variable degrees of biological control on Mg ions during biomineralisation. Understanding this biological control is essential for developing proxies based on biogenic carbonates.

Methods: In this work, we present a new approach of measuring Mg isotopes in biogenic carbonates using Laser Ablation Multi-Collector Inductively Coupled Plasma Mass Spectrometry (LA-MC-ICPMS).

Results: Our results show that this microanalytical approach provides relatively fast, high spatial resolution (<0.2 μm) measurements with high precision and accuracy down to 0.2‰ (2SE). To achieve high levels of precision and accuracy, baseline interferences need to be monitored and a carbonate standard with a relatively low trace metal composition similar to biogenic carbonates should be used. We also demonstrate that the matrix effect on Mg isotopes in carbonates with low Fe and Mn is limited to less than 0.2‰ fractionation under different laser parameters and low oxide condition (<0.3% ThO/Th).

Conclusions: Our newly developed LA-MC-ICPMS method and its applications to biogenic carbonates show significant advantages provided by the microanalytical approach in understanding complex processes of biomineralisation in marine calcifiers.

1 | INTRODUCTION

Next to oxygen, magnesium is the most common rock-forming element abundant in the earth's crust and as a cation in seawater.¹ Magnesium has three stable isotopes, ²⁴Mg, ²⁵Mg and ²⁶Mg. The large relative mass differences between these isotopes make the Mg isotope system a powerful tool in tracking both high- and low-temperature fractionation mechanisms related to geochemical and biological processes.^{2–6} The last two decades have witnessed a large

increase in studies and application of Mg isotopes in geochemistry including attempts to utilise them to understand the biomineralisation processes of marine calcifiers.^{7–9} Mg isotope studies usually define changes in isotope ratio on the $\delta^{26}\text{Mg}$ scale,³ and biological carbonates display relatively large, ~5‰, variation in $\delta^{26}\text{Mg}$ values, which is attributed to variable degrees of biological control of Mg ions during calcification.^{7,10} For example, modern planktonic foraminifera have very low isotopic signatures (e.g. –4‰ compared with $\delta^{26}\text{Mg}_{\text{seawater}}$ of –0.8‰) accompanied by Mg/Ca elemental ratios that

are an order of magnitude lower (0.5 mmol/mol) than that of inorganic calcite precipitated from seawater,¹¹ whereas the $\delta^{26}\text{Mg}$ values of benthic foraminifera are around -2‰ and have significantly higher Mg/Ca ratios (150 mmol/mol).¹² While various mechanisms have been proposed to explain this range in foraminiferal Mg/Ca ratios,^{13,14} none of these biomineralisation models can account for the associated range in Mg isotopic compositions. Similar to foraminifera, the Mg isotope signatures of the aragonitic skeleton of modern corals have been linked to internal biomineralisation processes.¹⁵ Annual variations of $\sim 0.2\text{‰}$ in $\delta^{26}\text{Mg}$ values found in reef-building colonies of *Porites* coral from the Great Barrier Reef (GBR) were attributed to light-enhanced calcification during summer periods.¹⁶ Despite these few pioneering studies, the application of Mg isotopes to biomineralisation is still limited due to the analytically challenging and labour-intensive methods employed in measuring Mg isotopes.

The majority of Mg isotope measurements employ solution-based methods to study geological or biological samples where cation-exchange column(s) are used to remove all the impurities from the Mg-containing solution.^{17–19} The 'purified' solution is then measured by Multi-Collector Inductively Coupled Plasma Mass Spectrometry (MC-ICPMS) relative to a well-characterised bracketing standard, with analytical uncertainties of 0.03‰ (2SD) or less being obtained.^{18,20,21} These methods are very precise but also very labour-intensive as the removal of matrix ions is a complex and challenging task.²² The other limitation of solution-based methods is the relatively large sample volume required for analyses, which often restricts measurements to a 'bulk' approach instead of the high-resolution spatially controlled analyses required to understand biomineralisation processes with large physiologically controlled spatial/temporal variability.

Microanalytical measurements using Secondary Ion Mass spectrometry (SIMS) or Laser Ablation (LA)-MC-ICPMS provide alternative ways of measuring Mg isotopes.^{17,23} These *in situ* techniques are capable of delivering geochemical data with sub-micron resolution.^{24–26} Recent developments in large geometry SIMS instruments equipped with multi-ion collection technology have yielded results comparable in precision and accuracy with solution-based methods in samples with a Mg concentration of several percent.²⁷ However, both SIMS and, as will be described, LA-MC-ICPMS applications are subject to significant matrix effects potentially compromising the accuracy of Mg isotope measurements.^{24,25} For example, a deviation of up to 2‰ from true values has been reported in synthetic olivines, with identical $\delta^{26}\text{Mg}$ values but different Mg concentrations, analysed by LA-MC-ICPMS.^{28,29} This and other matrix effects have been attributed to fractionation induced during either plasma ionisation or laser ablation.²⁹ However, none of these microanalytical techniques have been applied to measure Mg isotopes in biogenic carbonates.

The focus of this study is to apply LA-MC-ICPMS to measure Mg isotopes in biogenic carbonates and understand the applicability of this microanalytical technique to problems of biomineralisation, and the limitations of this technique. We used a series of experiments on inorganic carbonates to investigate the effects of the analytical setup and matrix on the precision and accuracy of $\delta^{26}\text{Mg}$ measurements.

This work is based on our progress over the last five years in monitoring and optimising analytical protocols for Mg isotope measurements in carbonates. In addition, we applied this optimised analytical method to characterise the distribution of Mg isotopes within individual foraminifera shells and coral skeletons and to assess the applicability and advantages of *in situ* measurements.

2 | EXPERIMENT

2.1 | Analytical setup

Magnesium isotope measurements were performed using a Neptune Plus™ double-focusing multi-collector inductively coupled plasma mass spectrometer (Thermo Scientific, Bremen, Germany) coupled with a G2 Analyte™ Laser Ablation system (Teledyne, Bozeman, MT, USA). The data presented in this paper is a combination of measurements obtained in three different setups at the University of Cambridge, the University of Western Australia and the Thermo Scientific factory in Bremen, Germany, during twenty-four analytical sessions conducted over the last five years. All three setups include exactly the same instrumental configuration and were independently optimised to the same extent to minimise oxide production and improve signal stability by employing an in-house built smoothing device (Squid) with O-ring and Swagelok® gas connectors.

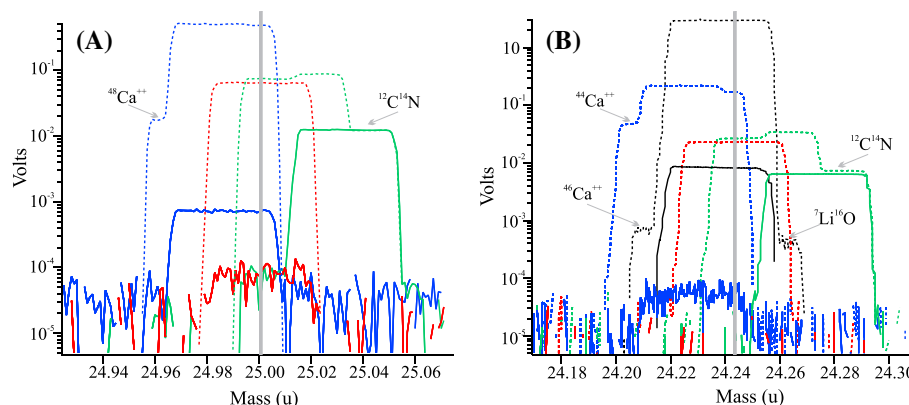
The Laser Ablation system was fitted with a two-volume ablation chamber and was run at 1 L/min He flow with 0.8 mL/min N_2 addition. Parameters of the laser ablation, such as fluence, frequency and spot size, were modified during different analytical runs to check their effect on Mg isotope fractionation (more details in section 3).

All three LA-MC-ICPMS systems utilised in this study were equipped with a jet interface and were run with an X-skimmer and Jet-sample cones to maximise sensitivity in the laser ablation mode. Two different cup configurations were used: 'traditional' with H3, C and L3 cups dedicated to the 24, 25 and 26 Mg isotopes, respectively (Figure 1A) and 'Na-configuration' where H3 was set for the Na mass and H1, L2 and L4 for the Mg isotopes (Figure 1B). The Faraday-cup measurements were performed using $10^{11} \Omega$ resistors for the cup amplifiers for all collectors. The MC-ICP mass spectrometer was run in high-resolution mode ($m/\Delta m \sim 8000$) to resolve polyatomic interferences. Large interferences were found related to ^{48}Ca doubly charged ions on mass 24 and $^{12}\text{C}^{14}\text{N}$ on mass 26, which were resolvable using high resolution. Na measurements were primarily undertaken to minimise production of Na scattered ions (see section 3.1) in the collector region and they were not used in Mg isotope calculations. The terminology and calculation were from Young and Galy³ and all values were reported in ‰ on the DSM scale.

2.2 | Standards and samples

To quantify the precision and accuracy of Mg isotope measurements using LA-MC-ICPMS we used a series of in-house carbonate

FIGURE 1 Mass scans for magnesium isotopes during ablation of NIST610 glass (dashed lines) and gas blanks (solid lines) for the two-cup configuration during A) traditional set up with the H3 cup for ^{24}Mg (blue), the C cup for ^{25}Mg (red) and the L3 cup for ^{26}Mg (green) and B) Na cup configuration with H3 cup for Na (black), H1 cup for ^{24}Mg (blue), L2 cup for ^{25}Mg (red) and L4 cup for ^{26}Mg (green). Vertical grey line corresponds to the collection interval position to avoid major interferences from polyatomic and doubly charged ions [Color figure can be viewed at wileyonlinelibrary.com]



standards and internationally recognised reference materials with known $\delta^{26}\text{Mg}$ values such as JCT.^{9,12,30,31} All in-house carbonates were first measured in solution mode to quantify their Mg isotope ratios relative to the DSM-3 (Dead Sea Magnesium after Galy et al.²⁰) reference material. The solution measurements were undertaken using a one-step elution method as described by Bohlin et al.³² and a standard-sample-bracketing (SSB) approach using DSM-3 as the primary standard and Cambridge-1 as a secondary standard. The reproducibility of Cambridge-1 was $\delta^{26}\text{Mg} = -2.63\text{‰}$ with ± 0.08 (2SD) reproducibility over the duration of two analytical sessions. Details of the solution method used here can be found in Bohlin et al.³² In laser ablation mode, sodium reference glasses, NIST610 and 612, were used to tune the mass spectrometer and to evaluate changes in baseline and interferences (Figure 1). The Mg/Ca ratios and $\delta^{26}\text{Mg}$ values of the reference material used in this work are summarised in Table 1.

To demonstrate the applicability of our *in situ* Mg isotope method to carbonate biomineralisation, we studied two types of marine biogenic carbonates. The first set was a collection of calcitic shells of the planktonic foraminifera *Orbulina universa* picked from the core-top sediment sample Sonne-18496 from the North West Australian margin.³³ The *O. universa* shells were broken into fragments and ultrasonicated in methanol until all detrital contamination visible

under a stereomicroscope had been removed. Each fragment was mounted on carbon tape with the inner surface facing up to increase spatial resolution during laser ablation. To minimise the effect of surface contamination, the outer $0.5\text{ }\mu\text{m}$ of calcite of each foraminifera was pre-ablated.³⁴

The second biogenic carbonate used in our method application is the aragonite skeleton of a *Porites* coral collected in the inshore region of the central Great Barrier Reef.³⁵ We analysed a 5-year-long section of this *Porites*, which represents coral growth from 1996 to 2001 and covers a period of thermal-stress-induced bleaching in 1998. This coral interval has been previously studied for trace metal and boron isotope geochemistry (see details in D'Olive and McCulloch³⁵). For Mg isotope analyses, we selected two sections, each $\sim 2.5\text{ cm}$ long, corresponding to path-C described in the study of D'Olive and McCulloch.³⁵ Prior to analyses, these sections were cut into 1-cm-thick by 2-cm-wide slabs and were cleaned in deionised water using an ultrasonic bath for 5 min with quick 10-s rinse in methanol. The surface of each ablation track was also precleaned by removing $\sim 0.5\text{ mm}$ of the surface skeleton using laser ablation with the following settings: 15 Hz with $50\text{ }\mu\text{m/s}$ track speed and $250 \times 100\text{ }\mu\text{m}$ spot size. This amount of pre-ablation was performed to remove any potential contamination from the porous skeleton of corals.

TABLE 1 Summary of magnesium isotope and Mg/Ca ratios for our in-house collection of carbonate reference materials used in this study. Values are based on solution measurements with 3–6 replicates (for details, see section 2)

#	Lab name	Mineral/composition	Comments	$\delta^{26}\text{Mg}$ value ‰	$\pm 2\text{SE}$ ‰	Mg/Ca mmol/mol
1	eBlue	Inorganic calcite monocrystal	Primary standard, from an esoteric online shop	−4.32	0.05	3.2
2	NCC	Inorganic calcite monocrystal	High Mn and Fe standard, from collection of T. Dickson	−3.89	0.04	12.2
3	LFC	Inorganic calcite monocrystal	Low Mg standard, from collection of T. Dickson	−4.79	0.05	1.7
4	eYel	Inorganic calcite monocrystal	High Mg standard, from an esoteric online shop	−3.83	0.11	37.1
5	OKA	Inorganic calcite monocrystal	Carbonatite from Oka complex, Quebec, from collection of R. Gabitov	−0.93	0.11	3.5
6	JCT	Tridacna powder, pressed nano-pellet	Tridacna powder, pressed nano-pellet	−2.8	0.05	1.2

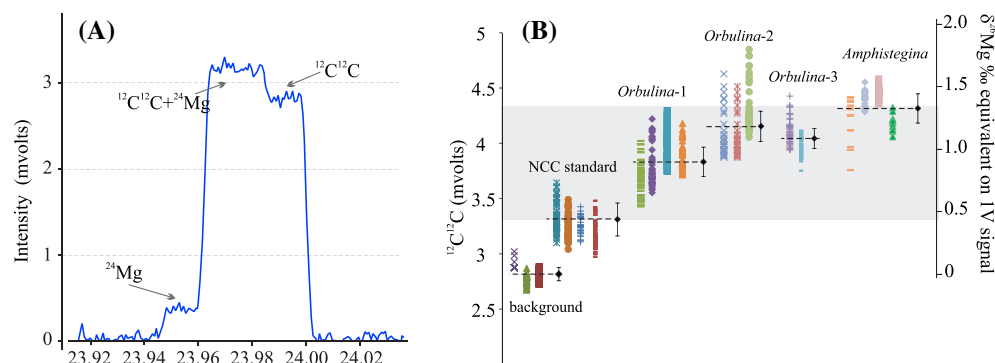


FIGURE 2 A, Mass scan of ^{24}Mg and presence of $^{12}\text{C}^{12}\text{C}$ on the right shoulder of the ^{24}Mg peak on the gas blank with 'leaky' laser ablation system. B, Contribution of $^{12}\text{C}^{12}\text{C}$ interference on the accuracy of Mg isotope measurements. The $^{12}\text{C}^{12}\text{C}$ intensity was measured on the right shoulder (free of magnesium) for gas blank (laser off – Background values), NCC standard, three low-Mg (*Orbulina*) and one high-Mg (*Amphistegina*) biogenic calcite. Coloured symbols are raw data for 2-s integrations during 20 s of ablation including several repeats on the same sample/gas blank. Black circles with error bars represent the combined averages for each sample/gas blank ± 1 standard error of the mean. The intensity is recalculated to ‰ $\delta^{26}\text{Mg}$ values assuming that the ^{24}Mg signal is 1 V (right vertical axis)

3 | RESULTS AND DISCUSSION

3.1 | Mass interferences

Calcium carbonate matrices pose additional challenges for Mg isotope measurements due to the considerable presence of doubly charged $^{48}\text{Ca}^{++}$ and $^{12}\text{C}^{12}\text{C}$ polyatomic species. The signal from $^{48}\text{Ca}^{++}$ can be $\sim 1/3$ of the ^{24}Mg intensity, and therefore separating these polyatomic species is critical in analysing biogenic carbonates. In high-resolution mode, the Neptune Plus™ can resolve the $^{48}\text{Ca}^{++}$ interference from ^{24}Mg on a narrow, 0.05 m/z unit window on the right shoulder of mass 24. Because of this relatively narrow collection window careful attention is required to the mass centring throughout the analytical session to minimise the possibility of the mass spectrometer drifting away from the interference-free part of the shoulder position. The $^{12}\text{C}^{12}\text{C}$ polyatomic interference was observed only during two analytical sessions where minor air leaks occurred in the gas lines of the laser system. These leaks were not obvious during the initial setup of the Neptune Plus and were only observed while monitoring Th/ThO, which was around 40%. The signal from $^{12}\text{C}^{12}\text{C}$ is visible on the right shoulder of the ^{24}Mg mass (Figure 2), which is on the opposite side to the $^{48}\text{Ca}^{++}$ interference (i.e. the left side of the ^{24}Mg mass). While high-resolution operation allows the $^{12}\text{C}^{12}\text{C}$ interference to be resolved from ^{24}Mg , it cannot be resolved at the same time as interferences from $^{48}\text{Ca}^{++}$ because of its location on the opposite side of the ^{24}Mg mass (Figure 2). To quantify $^{12}\text{C}^{12}\text{C}$ during ablation we set up a collection interval on the right shoulder of the ^{24}Mg mass in dynamic mode (jumping between collection positions). The gas background has a stable $^{12}\text{C}^{12}\text{C}$ signal of ~ 2.7 mV but this

can increase up to 4.5 mV during ablation of carbonates (Figure 2B). It also varies between different types of carbonates (e.g. biogenic and inorganic), potentially contributing up to 1‰ bias in $\delta^{26}\text{Mg}$ values on a 1-V signal of ^{24}Mg . Therefore, it is important to monitor the presence of $^{12}\text{C}^{12}\text{C}$ and to ensure that all gas fittings are leak free before undertaking Mg isotope measurements.

Another potential interference on Mg masses comes from scattered ions. Sodium (m/z 23) and Al (m/z 27) masses are adjacent to the Mg mass window and reflection of the Na ion has been observed with the 'traditional' collector configuration (see section 2.1). Na has a high ionisation energy and its signal can reach up to several tens of volts during the ablation of biogenic carbonates and hundreds of volts during the ablation of Na-rich matrices such as NIST610 and 612 glasses. The tail from ~ 100 V signal during NIST610 ablation is clearly visible during mass scans (Figure 1B) and it can contribute ~ 100 μV on the neighbouring detector of ^{24}Mg . However, the most important impact from scattered Na ions is related to negative baselines, which were observed on all masses due to the presence of these Na scattered ions across the Faraday-cup collection assembly (Figure 3). The results from the conventional cup configuration (Figure 1A) with H3, C and L3 cups are significantly affected by reflected Na ions. The negative baselines can reach up to -3 mV and vary in intensity and location as the H4 cup is moved, confirming their origin from reflection around the Na mass (Figures 3A and 3B). These negative baselines are only present during the ablation of Na-rich matrices and are probably dependent on the mass spectrometer cup configurations. For example, the Neptune Plus at the University of Cambridge has significantly smaller negative baselines than the Neptune Plus at UWA. This is probably due to the

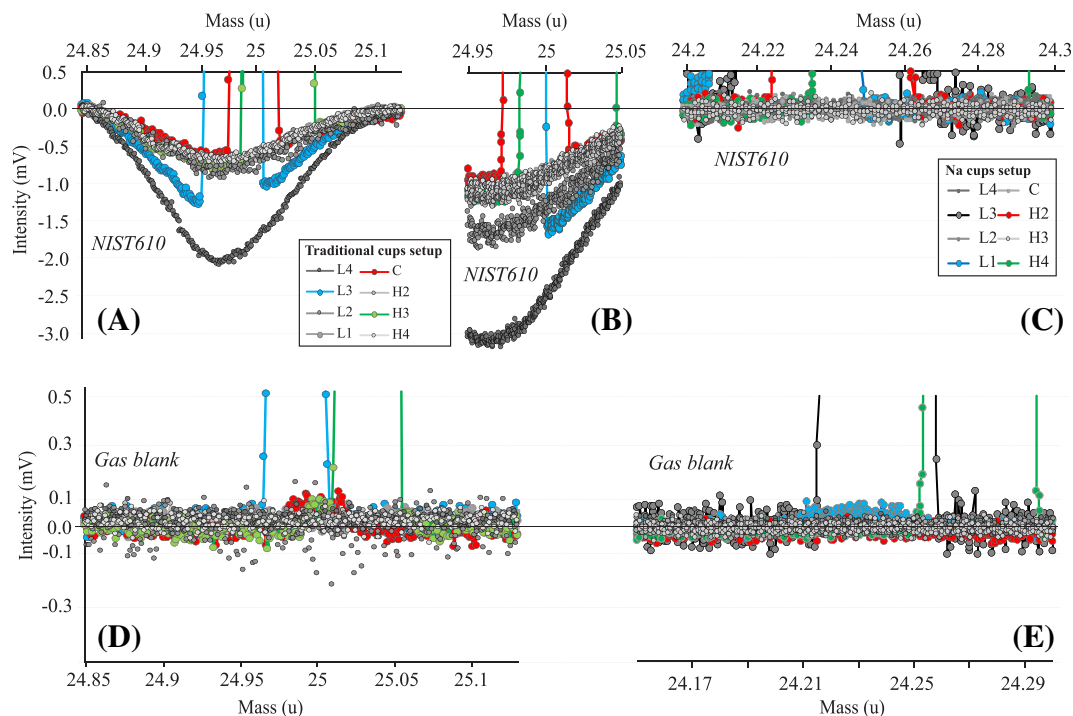


FIGURE 3 Mass scans around magnesium with focus on the distribution signal intensities close to baseline values. Mass scans were collected on all five cups during A–C, ablation of NIST610 glass, and D–E, gas blank measurements. A, B and D show the distribution of baselines for the ‘traditional’ cup configuration (see text and Figure 1). Note the negative values (A, B) during the ablation of the Na-rich glass standard. Scans A and B differed in the position of the H4 cup which was moved by 0.2 u, resulting in a change in the absolute values of the negative baseline and their location relative to the Mg masses (coloured lines). There are no negative baselines during gas blank measurements, linking them to Na scattered ions. C and E show the distribution of baselines for ‘Na’ cup configuration (see text and Figure 1). Note the change in scale compared with the top panel (A–C) and minimal variation of baseline for both NIST610 ablation and gas blank measurements

presence of CDD ion counters on H4 and L4 in the UWA setup. To overcome this, we used a ‘Na cup configuration’ to minimise scattered ions by effectively trapping Na in the H3 collector (Figure 1B). This configuration minimised the variation in baseline to microvolt levels (Figures 3D and 3E), which can arguably be neglected for Mg isotope measurements. It is interesting to notice here that in our initial studies without the Na cup configuration we found ~25% changes in $\delta^{26}\text{Mg}$ values of NIST612 glass with increasing laser spot size (Figure S1, supporting information), which was clearly an artefact of Na scattered ions on Mg masses. A similar trend has been previously reported in Na-rich samples, interpreted as a ‘laser-induced’ matrix effect.^{28,36} Although these reported changes were not necessarily related to scattered Na ions, it underlines the importance of monitoring baseline variations during ablation as an essential component of the Mg isotope analytical setup.

3.2 | Matrix effect

We designed a series of experiments to investigate the effect of plasma loading as well as Mg fractionation at the ablation site. The first experiment included measurement of the $\delta^{26}\text{Mg}$ value of a homogeneous standard of known isotopic composition (NCC, see Table 1) using different laser spot sizes (50, 65, 80, 95 and 110 μm),

laser frequency (2, 3, 4 and 6 Hz) and laser fluency at the ablation site (0.9, 1.2 and 1.5 J/cm^2). The analytical session for this experiment included measurements with each laser parameter repeated twice to minimise the effect of instrument drift. Our data have been regressed against the same NCC standard ablated with 5 Hz, 1.2 J/cm^2 and spot size 80 μm using three samples in the standard bracketing approach. For example, to check the effect of spot size, the ablation sequence included NCC_{std} (3 repetitions) \rightarrow $\text{NCC}_{\text{spot size-50}}$ (3 repetitions) \rightarrow NCC_{std} (3 repetitions) \rightarrow $\text{NCC}_{\text{spot size-65}}$ (3 repetitions) \rightarrow NCC_{std} (3 repetitions) \rightarrow $\text{NCC}_{\text{spot size-80}}$ (3 repetitions), and so on. This sequence is repeated at the end of the sequence (76 measurements + std). To limit the effect of down-hole fractionation and to obtain the same ablation pit depth we fired the laser for 100 shots regardless of other laser parameters. The error in $\delta^{26}\text{Mg}$ values was calculated as the pooled 2SE from repeated measurements of each investigated parameter.

The results from the first experiment demonstrate the distinct impact of laser parameters on Mg fractionation (Figure 4A). Both laser density and frequency have minimal effect on the $\delta^{26}\text{Mg}$ value, well within measurement uncertainty (green and red spots on Figure 4A). The size of the laser spot, on the other hand, has a strong negative correlation with $\delta^{26}\text{Mg}$ values with a decrease of 2.7% when changing the spot size from 50 to 125 μm . This means that a 3-fold increase in material delivered to the plasma (volts (V) on

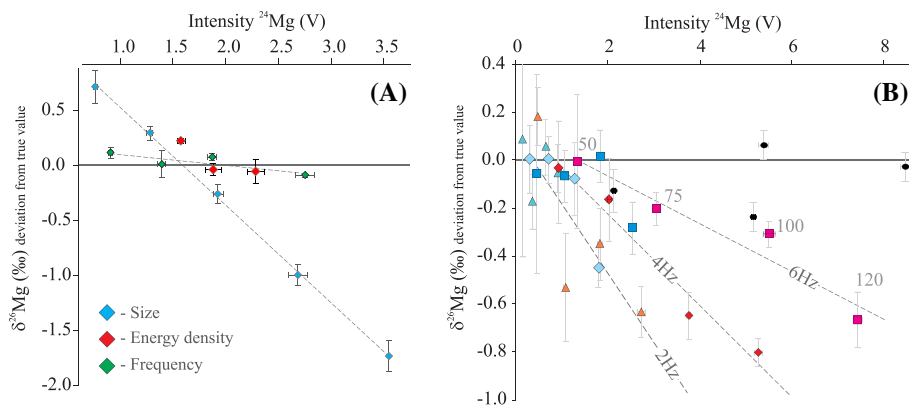


FIGURE 4 Effect of sample matrix on the accuracy of $\delta^{26}\text{Mg}$ measurements in carbonates. A, Results of the first experiment (more details in section 3.2) where the offset of measured $\delta^{26}\text{Mg}$ values from the standard true values is compared for laser spot size (blue diamonds), laser fluency (red diamonds) and laser frequency (green diamonds). Note the minimal change in the $\delta^{26}\text{Mg}$ offset for both frequency and fluency but the strong negative correlation with the $\delta^{26}\text{Mg}$ offset with laser spot size, resulting in $>2.5\%$ instrumental bias. B, Results of the second experiment where the same $\delta^{26}\text{Mg}$ offset for calcitic standards with different Mg concentrations is investigated. Blue symbols are data for OKA carbonatite which has a similar Mg concentration to the primary standard. Red symbols are data for NCC standard with $\sim 1\%$ Fe and black circles are data for high-Mg standard eYel. Both NCC and OKA were ablated with 6 Hz (squares), 4 Hz (diamonds) and 2 Hz (triangles), with different spot sizes marked as dashed lines for each frequency. Note the lack of patterns in fractionation except in the NCC standard data where a negative correlation exists between laser spot size and $\delta^{26}\text{Mg}$ offset. Grey error bars on both plots A and B represent 2 standard error intervals

Figure 4A) resulted in only a $\sim 0.2\%$ shift in values as the frequency of the laser was changed, but this was equivalent to $\sim 1.7\%$ when a similar plasma loading was achieved by changing the laser spot size from 50 to 100 μm . Similar effects have been previously observed for synthetic olivines²⁹ and silica references glasses.^{25,29} These studies reported little change in Mg fractionation with changing laser density or frequency. This strongly suggests that the observed Mg isotope fractionation with increase in spot size occurs at the ablation site and is not related to processes within the plasma (e.g. partial ionisation, mass-charge effect, and others) or particle transport. Norman et al²⁹ attributed this effect to down-hole fractionation. Our laser pits were also only $\sim 10\ \mu\text{m}$ deep, which is shallower than in previous studies (e.g. three times shallower than in the work of Norman et al²⁹) and the $\delta^{26}\text{Mg}$ values did not change as the laser drilled deeper into the sample. Therefore, down-hole fractionation can be excluded as a potential source of the observed changes in $\delta^{26}\text{Mg}$ in our study. Unlike in Norman et al,²⁹ we also corrected all our data for amplifier responses, or τ -correction,³⁷ which further reduced the possibility that the observed $\sim 1.7\%$ change in $\delta^{26}\text{Mg}$ values is an analytical artifact.

A second experiment was conducted to investigate if the matrix effect on Mg fractionation is present in standards with different Mg and trace metal concentrations and to further understand $\delta^{26}\text{Mg}$ changes with ablation spot size. In this experiment three standards,

NCC, OKA and eBlue, were measured under different ablation conditions. The composition of the primary standard, eBlue, is similar to that of natural biogenic calcite (see Table 1). Similar to the first experiment, we made triplicate measurements per standard and repeated the cycle in all standards three times (e.g. each standard was measured 9 times at each laser parameter). Only frequency (2, 4 and 6 Hz) and spot size (50, 75, 100 and 120 μm) were varied in this experiment. The critical difference in the second experiment is that the primary standard (eBlue) was always ablated with the same laser parameter as the sample being investigated. This can be considered a 'true' matrix test as the standard and sample only differed in their matrix composition (e.g. Mg and other trace element concentrations). The results of the second experiment were significantly different from those in the first experiment, with a much smaller Mg fractionation with varying laser spot size and frequency observed in the second experiment (Figure 4B). Deviations from true $\delta^{26}\text{Mg}$ values are statistically significant only for the NCC standard, which shows a similar negative correlation to that in the first experiment with laser spot size (Figure 4B). These deviations for NCC, however, were also 2.5-times smaller when NCC was referred, that is used as the primary standard, to itself in the previous experiment (Figure 4A). In contrast, all except one data point for the OKA standard were within 0.2% of the expected $\delta^{26}\text{Mg}$ value (blue point in Figure 4B). OKA and eBlue have similar Mg concentrations, which are four times lower than in

the NCC standard. Therefore, the Mg concentration could be the reason for the observed differences in Mg fractionation in the OKA and NCC standards. This would be consistent with the olivine study as reported in Norman et al.²⁹ To check this hypothesis, we added eYel, a calcitic standard which has a Mg content three times higher than NCC and approximately ten times higher than eBlue. This standard was measured against eBlue as the primary standard using laser spot sizes of 85, 110 and 130 μm . Surprisingly, the laser-induced offset of this high-Mg calcite was within 0.2‰ of its true value (black circles on Figure 4B). Therefore, we can conclude that the correlation between laser spot size and $\delta^{26}\text{Mg}$ value is unique for the NCC standard. The fractionation reported here for NCC follows the terrestrial fractionation line in the three-isotope plot, and the $\Delta^{26}\text{Mg}$ value (as defined by Young and Galey³) is within error of zero for NCC and all other measured standards. Currently, we do not have a conclusive explanation for this phenomenon but this matrix-related offset in the NCC standard is strongly related to oxide levels during the analytical session (discussed in the next section). The NCC standard also contains $\sim 1\%$ Fe and it has relatively high Mn concentrations so we speculate that the presence of Fe during ablation is responsible for the observed Mg fractionation. This may also explain why nearly identical behaviour was reported in olivines, which are also rich in Fe. This Fe-induced bias is well known in SIMS studies where Fe content is routinely used to correct for instrument mass bias on carbon,^{38,39} oxygen^{40,41} and lithium isotopes.⁴² Although this analogy may not be applicable to laser ablation, it is also known that electromagnetic properties of carbonate minerals vary with Fe + Mn content.^{38,43–45} It is possible that the Fe content affects the ablation property of carbonates or the formation of Mg-Fe oxides, which later alter Mg fractionation during ablation.

3.3 | Accuracy and precision of $\delta^{26}\text{Mg}$ measurements in carbonates using LA-MC-ICPMS

We demonstrated that matrix-induced fractionation in calcium carbonate is limited to $\pm 0.2\text{‰}$ unless samples have significant Fe or Mn content. The precision of primary and secondary standard measurements mainly depends on the duration of the analyses and can be as small as $\pm 0.03\text{‰}$ (2SE) within one analytical session. However, the session-to-session variability (i.e. external variability) is significantly higher (Figure 5). We also noticed that oxide levels directly affect the variability of the secondary standard and the offset from true values (i.e. accuracy). We therefore tuned the mass spectrometer to $<0.3\%$ ThO/Th ratio as a standard routine for each analytical session. The typical accuracy of secondary standards within sessions with low oxide is on average $\pm 0.2\text{‰}$ (2SE). Further improvement in method accuracy is limited by the variability of $\delta^{26}\text{Mg}$ values within our standards. This level of method accuracy is certainly well below the current standards for Mg isotope measurements using the conventional solution method. However, our method is the only available microanalytical approach in carbonates that can deliver accuracy to $\pm 0.2\text{‰}$ Mg isotope measurements with sub-micron

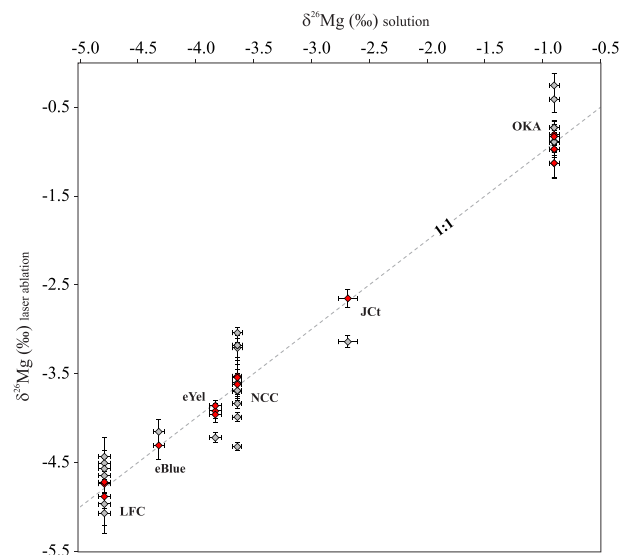


FIGURE 5 Accuracy of LA-MC-ICPMS magnesium isotope measurements compared with solution-based data. Grey diamonds are laser ablation measurements for analytical session tuned for relatively high oxide rates (ThO/Th $>0.3\%$) and red diamonds are for measurements with low oxide tuning (ThO/Th $<0.3\%$). Note the relatively large spread, up to 0.7‰, in LA-MC-ICPMS data from high-oxide sessions (grey diamonds). Error bars represent ± 2 standard error intervals

resolution. In the next section we will show that this method opens new avenues in biomineralisation studies and can potentially help elucidate complex biogeochemical processes behind biomineral formation.

4 | APPLICATIONS

4.1 | Sub-micron Mg isotope distribution within individual shells of planktonic foraminifera

Foraminiferal biomineralisation has been a topic of debate for at least the last 50 years because of the use of foraminiferal geochemistry as a tracer for environmental parameters.^{46,47} For example, the Mg/Ca value of planktonic foraminifera is one of the most commonly-used proxies for reconstructing seawater temperature.^{48,49} However, the reliability of this proxy, especially in reconstructing ancient oceans with different Mg concentrations, has been questionable due to the strong biological control on Mg incorporation in foraminifera. It is estimated that planktonic foraminifera remove $\sim 99\%$ of Mg from seawater during biomineralisation.^{14,50} Moreover, some foraminifera, such as *Orbulina universa*, have large diurnal Mg/Ca variability within individual shells,^{51–53} which arguably needs to be understood to improve the reliability of temperatures derived from Mg/Ca paleothermometry.³⁴

Here, we applied our microanalytical method to measure Mg isotopes in shells of the planktonic foraminifera *O. universa*. Five well-preserved shells were picked from a sediment sample and mounted

on carbon tape as fragments oriented with the inner side of the shells facing up. Each shell was measured three times to document variability in Mg isotope ratios and method reproducibility. Data were collected simultaneously as the laser ablated through the foraminiferal shells. We used the following laser parameters: square 80 μm spot size, 2 Hz frequency and 1.2 J/cm² fluency. The Mg/Ca values were estimated from the ²⁴Mg signal intensity using known Mg/Ca values of standards and with the assumption that [Ca] in our samples is the same as in our primary standard. Because of this assumption the Mg/Ca estimates may be offset from the true Mg/Ca values by a constant factor, which is the difference in [Ca] between standard and unknown, leading to ~15% inaccuracy. This value is insignificant for the purpose of our measurements, which is to compare Mg/Ca values of samples with an identical matrix, that is, the same foraminifera shell. The results show the expected low- and high-Mg bands associated with daily cycles, each approximately 3 μm thick (Figure 6). The $\delta^{26}\text{Mg}$ values positively correlate with Mg/Ca values and range from -6 to -3.5‰ with ~1‰ change across the low- to high-Mg band. The Mg isotope ratios also show a gradual increase in values during shell ontogenesis, from inside to outside of the shell. Three tracks from different fragments of individual shells show good agreement, with most of the $\delta^{26}\text{Mg}$ values within 95% confidence interval of each other.

This range of $\delta^{26}\text{Mg}$ variability within individual *O. universa* shells is equivalent to the published results for all planktonic foraminifera.^{8,11} Such significant fractionation is a result of large variations during the day-night cycle in foraminiferal calcification.^{52,53} The night-time calcite is higher in Mg concentration and its isotope signature is closer to inorganic calcite $\delta^{26}\text{Mg}$ values, which are estimated to be around -3‰. Day calcite, on the other hand, has low Mg/Ca values and extremely low $\delta^{26}\text{Mg}$ isotope signatures (-6‰). However, it is also clear that the distribution patterns are not a simple mixture of two types of calcite, rather an effect of the biomineralisation mechanism, which operates at different rates during day and night periods. This mechanism also changes during ontogenesis as older (outer) layers typically have higher $\delta^{26}\text{Mg}$ values (Figure 6). The origin of this biomineralisation mechanism will be the subject of another study. In this work, we highlight the applicability of LA-MC-ICPMS in characterising sub-micron distributions of Mg isotopes within biogenic calcite and its major advantages in understanding the complex issues of biomineralisation compared with solution-based methods.

4.2 | Changes in Mg isotopes across a stress band in massive *Porites* coral and its relation to calcification rate

The geochemistry of massive *Porites* corals has been used to produce high-resolution paleoclimate records to understand seawater temperature variability, the evolution of monsoon systems,^{54,55} the El Niño-Southern Oscillation,⁵⁶ and other seasonal and inter-annual modes of climate variability.^{57,58} Recently, it has been suggested that

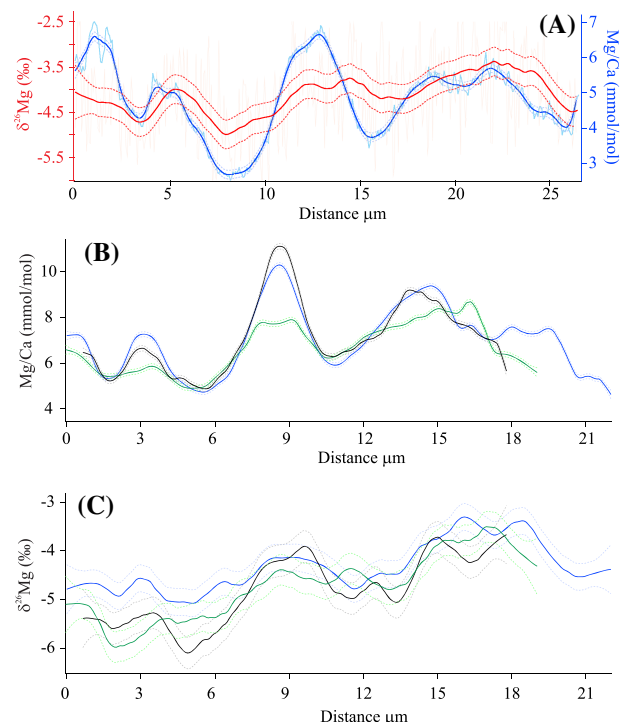


FIGURE 6 Distribution of Mg/Ca and $\delta^{26}\text{Mg}$ values across the shell wall of the planktonic foraminifera *Orbulina universa*. A, Covariance Mg/Ca (estimated from ²⁴Mg Volt intensity) and $\delta^{26}\text{Mg}$ values during ablation from the inner to the outer side of the shell. Pale red line corresponds to original $\delta^{26}\text{Mg}$ data, and the solid thick red line indicates 6-s smoothed $\delta^{26}\text{Mg}$ values using locally weighted regression (loess) bracketed by 95% confidence intervals (dashed lines). Similarly, original Mg/Ca values are shown by light blue lines, and solid blue represents smoothed Mg/Ca with 95% confidence intervals (dashed lines). B, C, Comparison between smoothed Mg/Ca (B) and $\delta^{26}\text{Mg}$ (C) data measured from different fragments of one shell. Dashed lines are 95% confidence intervals. Both Mg/Ca and $\delta^{26}\text{Mg}$ values show regular oscillation between the high Mg/Ca/ $\delta^{26}\text{Mg}$ band formed in calcification at night and the low-Mg/ $\delta^{26}\text{Mg}$ band formed during daytime. The distance in microns corresponds to the shell thickness, estimated from the ablation rate assuming 0.1 μm removal by each laser pulse. Zero in distance corresponds to the inner shell surface

coral geochemistry can be used to understand coral responses to heat waves and associated bleaching events.^{35,59,60} These events lead to substantial changes in coral physiology and reduction of calcification rate and can be seen in coral skeleton as 'stress bands'.^{61,62} In this study, we measured the Mg isotopes across one of these stress events as the second application for our new microanalytical method. The Mg isotopes were measured along two laser tracks at 9 $\mu\text{m/s}$, 5 Hz and rectangular, 45 \times 145 μm , beam size. One track was aligned along the axis of maximum growth and the other track followed the direction of growth of an individual coral polyp (Figure 7A). The same interval was previously analysed for boron and trace metal geochemistry³⁵ and these transects are on the same plane as path B and adjacent to path C in that study.

The magnesium isotope ratios along the central track changed from -1.9 to -1.6‰ across the 1998 bleaching interval and then

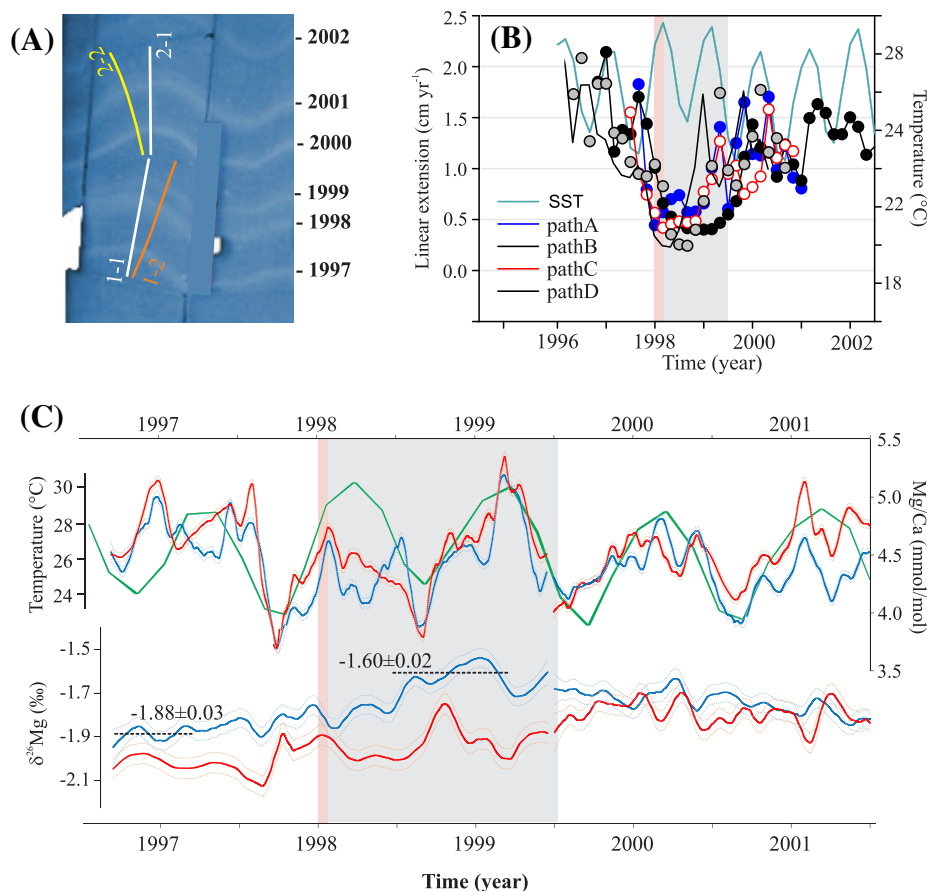


FIGURE 7 Effect of a coral bleaching event on *Porites* $\delta^{26}\text{Mg}$ values. A, Location of laser track relative to coral growth bands shown here as fluorescent bands, with the light blue band forming during summer. This section of the coral corresponds to coral growth from 1997 to 2002 (for more details, see D'Olive and McCulloch³⁵). Lines 1-1 and 2-1 are positioned along the axis of maximum extension/growth. Tracks 1-2 and 2-2 are located axially and along individual polyp growth. B, Changes in extension/calcification rate of the *Porites* colony measured along a different track and corresponding sea surface temperature (green line), modified from D'Olive and McCulloch³⁵. The C, Mg/Ca values are estimated from the ^{24}Mg intensity in volts (top panel) and the $\delta^{26}\text{Mg}$ values (bottom panel) measured across the *Porites* coral. Blue lines are bi-weekly smoothed (loess curve) values for tracks 1-1 and 2-1 (central on A) and red lines are smoothed values for laser tracks 1-2 and 2-2 (axial on A). The green line represents *in situ* sea-surface temperatures (data from D'Olive and McCulloch³⁵). Dashed lines are 95% confidence intervals. Pink and grey intervals on background of B and C correspond to the coral thermal bleaching event (pink) and stress band with low extension rates (grey)

returned to -1.9% around 2001 (Figure 7C). The 95% confidence interval for the average track values corresponds to $\pm 0.05\%$, which is significantly better than the uncertainty reported for spot analyses used in the foraminifera study. The main reason for this is the better counting statistics during track measurements where large numbers of individual measurements are averaged over a long (5 min) collection interval. However, despite the high measurement precision we cannot resolve seasonality in the Mg isotope ratios across the studied interval. This seasonality is clearly pronounced in the Mg/Ca values, which were estimated from the Mg intensity. It is possible that the lack of seasonal signal in $\delta^{26}\text{Mg}$ values, which was reported previously for *Porites* corals,¹⁶ is confounded by the presence of a stress band in our studied interval. The $\delta^{26}\text{Mg}$ values show a shift of 0.3% along the central track around mid-1997 with values reaching a maximum in the second half of 1998. This interval corresponds to the peak of bleaching and reduction in calcification rate (Figure 7B). The axial track shows significant deviation from the central track across the

bleaching interval (red profile on Figure 7C) with maximum deviation during the stress interval. The $\delta^{26}\text{Mg}$ values gradually return to the pre-bleaching background around 2001, two years after the stress event.

Our Mg isotope data present several implications for the biomineralisation processes of *Porites* coral during bleaching events. First, different parts of the coral responded in different degrees to the stress event. The central track or axis of maximum growth displayed more pronounced effects from the stress event than the axially located polyps. This corroborates the findings of D'Olive and McCulloch³⁵ using trace metal geochemistry. Second, our data imply a tight covariance of the coral calcification rate and the absolute $\delta^{26}\text{Mg}$ values. During the peak of coral bleaching the calcification rate dropped by $\sim 75\%$ and the Mg isotope ratios shifted toward inorganic aragonite values (e.g. $\delta^{26}\text{Mg} \sim 0.9\%$). We speculate that the biological machinery controlling the calcification rate directly influences Mg isotope ratios and that it was affected significantly as the coral is

presumed to have bleached and lost its symbiotic algae. The relationship between Mg isotope ratios and photosynthetic-enhanced coral calcification has been previously suggested to explain annual variation in $\delta^{26}\text{Mg}$ values of healthy *Porites*.¹⁶ Our data further supports this link and shows that heat-stress events affect the internal calcification machinery of the coral for several years. In our study it took two and a half years for the coral to repair its biomineralisation mechanisms. Therefore, it is not surprising that the recent frequent bleaching (e.g. three events in the last five years) devastated coral reef communities, particularly the Great Barrier Reef.^{63,64} Our data shows that the coral calcification machinery had insufficient time to recover and repair itself between frequent heat events leading to loss of coral cover and associated coral communities.

5 | CONCLUSIONS

Our LA-MC-ICPMS method for Mg isotope measurements in biogenic carbonates offers new advantages for biomineralisation studies. Here we have shown that accurate $\delta^{26}\text{Mg}$ measurements, up to 0.2‰, in biominerals can be achieved by removing doubly charged ion interferences arising from the carbonate matrix and by also avoiding scattered Na ions. Extensive investigation on the matrix effect on the accuracy of Mg isotope measurements using LA-MC-ICPMS revealed that the analytical bias in $\delta^{26}\text{Mg}$ values can be as high as 3‰ in carbonates that have significant (e.g. ~1% level) Fe or Mn content but can be limited to 0.2‰ in carbonates with low trace metal composition, which is typical in marine calcifiers. We also found a reduction in the matrix effect under low rates of oxide production in the plasma (<0.3% ThO/Th). Consequently, we recommend the use of matrix-matching standardisation for LA-MC-ICPMS measurements with careful attention being paid to the presence of oxides, doubly charged and scattered ions around Mg masses to improve the accuracy of this microanalytical method.

Applications of this new *in situ* method to biomineralisation studies show great potential. We have shown that sub-micron diurnal variability of $\delta^{26}\text{Mg}$ values in the planktonic foraminifera *O. universa* corresponds to layers of calcite formed during day-night cycles. We also found small but significant changes in $\delta^{26}\text{Mg}$ values in the aragonitic skeleton of *Porites* related to a coral bleaching event and reduced calcification. Using this LA-MC-ICPMS method that is capable of rapid measurements of Mg isotopes in biogenic carbonates with sub-micron resolution, these examples show new applications to further our understanding of biomineralisation studies. Furthermore, this method can be adapted to different types of biologic and inorganic carbonates, including speleothems and carbonatites, thereby covering a broader range of applications in geological studies.

ACKNOWLEDGEMENTS

This research was funded by ERC Advanced Grand (2010 NEWLOG ADG-267931) awarded to Prof. Harry Elderfield and also supported

by the ARC Centre of Excellence for Coral Reef Studies (CE140100020) and an ARC Laureate Fellowship (FL120100049) to MMC.

PEER REVIEW

The peer review history for this article is available at <https://publons.com/publon/10.1002/rcm.8918>.

ORCID

Aleksey Sadekov  <https://orcid.org/0000-0002-0436-0244>

Nicholas S. Lloyd  <https://orcid.org/0000-0002-1359-0551>

REFERENCES

1. Teng F-Z. Magnesium isotope geochemistry. *Rev Mineral Geochem.* 2017;82(1):219-287.
2. Guo B, Zhu X, Dong A, Yan B, Shi G, Zhao Z. Mg isotopic systematics and geochemical applications: A critical review. *J Asian Earth Sci.* 2019;176:368-385.
3. Young ED, Galy A. The isotope geochemistry and cosmochemistry of magnesium. *Rev Mineral Geochem.* 2004;55(1):197-230.
4. Tipper ET, Galy A, Bickle MJ. Riverine evidence for a fractionated reservoir of Ca and Mg on the continents: Implications for the oceanic Ca cycle. *Earth Planet Sci Lett.* 2006;247(3):267-279.
5. Handler MR, Baker JA, Schiller M, Bennett VC, Yaxley GM. Magnesium stable isotope composition of Earth's upper mantle. *Earth Planet Sci Lett.* 2009;282(1):306-313.
6. Schiller M, Handler MR, Baker JA. High-precision Mg isotopic systematics of bulk chondrites. *Earth Planet Sci Lett.* 2010;297(1):165-173.
7. Yoshimura T, Tanimizu M, Inoue M, Suzuki A, Iwasaki N, Kawahata H. Mg isotope fractionation in biogenic carbonates of deep-sea coral, benthic foraminifera, and hermatypic coral. *Anal Bioanal Chem.* 2011;401:2755. <https://doi.org/10.1007/s00216-011-5264-0>
8. Pogge von Strandmann PAE. Precise magnesium isotope measurements in core top planktic and benthic foraminifera. *Geochim Geophys Geosyst.* 2008;9:Q12015. <https://doi.org/10.1029/2008GC002209>
9. Hippler D, Buhl D, Witbaard R, Richter DK, Immenhauser A. Towards a better understanding of magnesium-isotope ratios from marine skeletal carbonates. *Geochim Cosmochim Acta.* 2009;73(20):6134-6146.
10. Eisenhauer A, Ba K, Böhm F. Marine calcification: An alkali earth metal isotope perspective. *Elements.* 2009;5(6):365-368.
11. Chang VTC, Williams RJP, Makishima A, Belshaw NS, O'Nions RK. Mg and Ca isotope fractionation during CaCO_3 biomineralisation. *Biochem Biophys Res Commun.* 2004;323(1):79-85.
12. Wombacher F, Eisenhauer A, Böhm F, et al. Magnesium stable isotope fractionation in marine biogenic calcite and aragonite. *Geochim Cosmochim Acta.* 2011;75(19):5797-5818.
13. Branson O, Redfern SAT, Tylliszczak T, et al. The coordination of Mg in foraminiferal calcite. *Earth Planet Sci Lett.* 2013;383:134-141.
14. de Nooijer LJ, Spero HJ, Erez J, Bijma J, Reichert GJ. Biomineralization in perforate foraminifera. *Earth Sci Rev.* 2014;135:48-58.
15. Saenger C, Wang Z. Magnesium isotope fractionation in biogenic and abiogenic carbonates: Implications for paleoenvironmental proxies. *Quat Sci Rev.* 2014;90:1-21.
16. Saenger C, Wang Z, Gaetani G, Cohen A, Lough JM. The influence of temperature and vital effects on magnesium isotope variability in *Porites* and *Astrangia* corals. *Chem Geol.* 2013;360-361:105-117.

17. An Y, Huang F. A review of mg isotope analytical methods by MC-ICP-MS. *J Earth Sci.* 2014;25(5):822-840.
18. Chang VTC, Makishima A, Belshaw NS, O'Nions RK. Purification of Mg from low-Mg biogenic carbonates for isotope ratio determination using multiple collector ICP-MS. *J Anal At Spectrom.* 2003;18(4):296-301.
19. Albarède F, Telouk P, Blichert-Toft J, Boyet M, Agranier A, Nelson B. Precise and accurate isotopic measurements using multiple-collector ICPMS. *Geochim Cosmochim Acta.* 2004;68(12):2725-2744.
20. Galy A, Yoffe O, Janney PE, et al. Magnesium isotope heterogeneity of the isotopic standard SRM980 and new reference materials for magnesium-isotope-ratio measurements. *J Anal At Spectrom.* 2003;18(11):1352-1356.
21. Galy A, Belshaw NS, Halicz L, O'Nions RK. High-precision measurement of magnesium isotopes by multiple-collector inductively coupled plasma mass spectrometry. *Int J Mass Spectrom.* 2001;208(1-3):89-98.
22. Choi MS, Ryu J-S, Lee S-W, Shin HS, Lee K-S. A revisited method for Mg purification and isotope analysis using cool-plasma MC-ICP-MS. *J Anal At Spectrom.* 2012;27(11):1955-1959.
23. Chaussidon M, Deng Z, Villeneuve J, et al. In situ analysis of non-traditional isotopes by SIMS and LA-MC-ICP-MS: Key aspects and the example of Mg isotopes in olivines and silicate glasses. *Rev Mineral Geochem.* 2017;82(1):127-163.
24. Fukuda K, Beard BL, Dunlap DR, et al. Magnesium isotope analysis of olivine and pyroxene by SIMS: Evaluation of matrix effects. *Chem Geol.* 2020;540:119482.
25. Oeser M, Weyer S, Horn I, Schuth S. High-precision Fe and Mg isotope ratios of silicate reference glasses determined in situ by femtosecond LA-MC-ICP-MS and by solution nebulisation MC-ICP-MS. *Geostand Geoanal Res.* 2014;38(3):311-328.
26. Xie L-W, Yin Q-Z, Yang J-H, Wu F-Y, Yang Y-H. High precision analysis of Mg isotopic composition in olivine by laser ablation MC-ICP-MS. *J Anal At Spectrom.* 2011;26(9):1773-1780.
27. Luu TH, Chaussidon M, Mishra RK, et al. High precision Mg isotope measurements of meteoritic samples by secondary ion mass spectrometry. *J Anal At Spectrom.* 2013;28(1):67-76.
28. Janney PE, Richter FM, Mendybaev RA, et al. Matrix effects in the analysis of Mg and Si isotope ratios in natural and synthetic glasses by laser ablation-multicollector ICPMS: A comparison of single- and double-focusing mass spectrometers. *Chem Geol.* 2011;281(1):26-40.
29. Norman MD, McCulloch MT, O'Neill HSC, Yaxley GM. Magnesium isotopic analysis of olivine by laser-ablation multi-collector ICP-MS: Composition dependent matrix effects and a comparison of the earth and moon. *J Anal At Spectrom.* 2006;21(1):50-54.
30. Tatzel M, Vogl J, Rosner M, Henahan MJ, Tütken T. Triple isotope fractionation exponents of elements measured by MC-ICP-MS – An example of Mg. *Anal Chem.* 2019;91(22):14314-14322.
31. Planchon F, Poulain C, Langlet D, Paulet Y-M, André L. Mg-isotopic fractionation in the manila clam (*Ruditapes philippinarum*): New insights into Mg incorporation pathway and calcification process of bivalves. *Geochim Cosmochim Acta.* 2013;121:374-397.
32. Bohlin MS, Misra S, Lloyd N, Elderfield H, Bickle MJ. High-precision determination of lithium and magnesium isotopes utilising single column separation and multi-collector inductively coupled plasma mass spectrometry. *Rapid Commun Mass Spectrom.* 2018;32(2):93-104.
33. Sadekov AY, Eggins SM, Klinkhammer GP, Rosenthal Y. Effects of seafloor and laboratory dissolution on the Mg/Ca composition of *Globigerinoides sacculifer* and *Orbulina universa* tests – a laser ablation ICPMS microanalysis perspective. *Earth Planet Sci Lett.* 2010;292(3-4):312-324.
34. Sadekov A, Eggins SM, De Deckker P, Kroon D. Uncertainties in seawater thermometry deriving from intratest and intertest Mg/Ca variability in *Globigerinoides ruber*. *Paleoceanography.* 2008;23:PA1215. <https://doi.org/10.1029/2007PA001452>
35. D'Olivo JP, McCulloch MT. Response of coral calcification and calcifying fluid composition to thermally induced bleaching stress. *Sci Rep.* 2017;7:2207. <https://doi.org/10.1038/s41598-017-02306-x>
36. Dai M-N, Bao Z-A, Chen K-Y, Yuan H-L. In situ analysis of Mg isotopic compositions of basalt glasses by femtosecond laser ablation multi-collector inductively coupled plasma mass spectrometry. *Chin J Anal Chem.* 2016;44(2):173-178.
37. Sadekov A, Lloyd NS, Misra S, Trotter J, D'Olivo J, McCulloch M. Accurate and precise microscale measurements of boron isotope ratios in calcium carbonates using laser ablation multicollector-ICPMS. *J Anal At Spectrom.* 2019;34(3):550-560.
38. Śliwiński MG, Kitajima K, Spiczka MJ, et al. SIMS bias on isotope ratios in Ca-Mg-Fe carbonates (part III): $\delta^{18}\text{O}$ and $\delta^{13}\text{C}$ matrix effects along the magnesite-siderite solid-solution series. *Geostand Geoanal Res.* 2018;42(1):49-76.
39. Śliwiński MG, Kitajima K, Kozdon R, et al. Secondary ion mass spectrometry bias on isotope ratios in dolomite-Ankerite, part II: $\delta^{13}\text{C}$ matrix effects. *Geostand Geoanal Res.* 2016;40(2):173-184.
40. Rollion-Bard C, Marin-Carbonne J. Determination of SIMS matrix effects on oxygen isotopic compositions in carbonates. *J Anal At Spectrom.* 2011;26(6):1285-1289.
41. Śliwiński MG, Kitajima K, Kozdon R, et al. Secondary ion mass spectrometry bias on isotope ratios in dolomite-Ankerite, part I: $\delta^{18}\text{O}$ matrix effects. *Geostand Geoanal Res.* 2016;40(2):157-172.
42. Bell DR, Hervig RL, Buseck PR, Aulbach S. Lithium isotope analysis of olivine by SIMS: Calibration of a matrix effect and application to magmatic phenocrysts. *Chem Geol.* 2009;258(1):5-16.
43. Rochette P. Inverse magnetic fabric in carbonate-bearing rocks. *Earth Planet Sci Lett.* 1988;90(2):229-237.
44. Telford WM, Geldart LP, Sheriff RE. Electrical properties of rocks and minerals. In: Geldart LP, Sheriff RE, Telford WM, eds. *Applied Geophysics*. Vol.2 Cambridge: Cambridge University Press; 1990:283-292.
45. Schmidt V, Hirt AM, Hametner K, Günther D. Magnetic anisotropy of carbonate minerals at room temperature and 77 K. *Am Mineral.* 2007;92(10):1673-1684.
46. Elderfield H. *The Oceans and Marine Geochemistry*. Oxford: Pergamon, Elsevier; 2006 Treatise on Geochemistry; No. 6.
47. Barker S, Cacho I, Benway HM, Tachikawa K. Planktonic foraminiferal Mg/Ca as a proxy for past oceanic temperatures: A methodological overview and data compilation for the last Glacial maximum. *Quat Sci Rev.* 2005;24(7-9):821-834.
48. Elderfield H, Bertram CJ, Erez J. A biomineralization model for the incorporation of trace elements into foraminiferal calcium carbonate. *Earth Planet Sci Lett.* 1996;142(3-4):409-423.
49. Elderfield H, Ganssen G. Past temperature and $\delta^{18}\text{O}$ of surface ocean waters inferred from foraminiferal mg/ca ratios. *Nature.* 2000;405(6785):442-445.
50. Nürnberg D, Bijma J, Hemleben C. Assessing the reliability of magnesium in foraminiferal calcite as a proxy for water mass temperatures. *Geochim Cosmochim Acta.* 1996;60(5):803-814.
51. Eggins S, Sadekov AY, De Deckker P. Modulation and daily banding of Mg/Ca in *Orbulina universa* tests by symbiont photosynthesis and respiration: A complication for seawater thermometry? *Earth Planet Sci Lett.* 2004;225:411-419.
52. Sadekov AY, Eggins SM, De Deckker P. Characterization of Mg/Ca distributions in planktonic foraminifera species by electron microprobe mapping. *Geochim Geophys Geosyst.* 2005;6:Q12P06. <https://doi.org/10.1029/2005GC000973>
53. Spero HJ, Eggins SM, Russell AD, Vetter L, Kilburn MR, Hönisch B. Timing and mechanism for intratest Mg/Ca variability in a living planktic foraminifer. *Earth Planet Sci Lett.* 2015;409:32-42.

54. Bryan SP, Hughen KA, Karnauskas KB, Farrar JT. Two hundred fifty years of reconstructed south Asian summer monsoon intensity and decadal-scale variability. *Geophys Res Lett*. 2019; 46(7):3927-3935.
55. Li X, Liu Y, Wu C-C, et al. Coral-inferred monsoon and biologically driven fractionation of offshore seawater rare earth elements in Beibu gulf, northern South China Sea. *Solid Earth Sci*. 2019;4(4): 131-141.
56. Carriquiry JD, Risk MJ, Schwarcz HP. Stable isotope geochemistry of corals from Costa Rica as proxy indicator of the EL Niño/southern oscillation (ENSO). *Geochim Cosmochim Acta*. 1994; 58(1):335-351.
57. Freund MB, Henley BJ, Karoly DJ, McGregor HV, Abram NJ, Dommenget D. Higher frequency of Central Pacific El Niño events in recent decades relative to past centuries. *Nat Geosci*. 2019;12(6): 450-455.
58. Abram NJ, Gagan MK, Liu Z, Hantoro WS, McCulloch MT, Suwargadi BW. Seasonal characteristics of the Indian Ocean dipole during the Holocene epoch. *Nature*. 2007;445(7125): 299-302.
59. Clarke H, D'Olivo JP, Conde M, Evans RD, McCulloch MT. Coral records of variable stress impacts and possible acclimatization to recent marine heat wave events on the northwest shelf of Australia. *Paleoceanogr Paleoclimatol*. 2019;34(11):1672-1688.
60. Hetzinger S, Pfeiffer M, Dullo WC, Zinke J, Garbe-Schönberg D. A change in coral extension rates and stable isotopes after El Niño-induced coral bleaching and regional stress events. *Sci Rep*. 2016;6: 32879. <https://doi.org/10.1038/srep32879>
61. DeCarlo TM, Cohen AL. Dissepiments, density bands and signatures of thermal stress in Porites skeletons. *Coral Reefs*. 2017;36(3): 749-761.
62. D'Olivo JP, McCulloch MT, Judd K. Long-term records of coral calcification across the central great barrier reef: Assessing the impacts of river runoff and climate change. *Coral Reefs*. 2013;32(4): 999-1012.
63. Hughes TP, Anderson KD, Connolly SR, et al. Spatial and temporal patterns of mass bleaching of corals in the Anthropocene. *Science*. 2018;359(6371):80-83.
64. Hughes TP, Kerry JT, Baird AH, et al. Global warming transforms coral reef assemblages. *Nature*. 2018;556(7702):492-496.

SUPPORTING INFORMATION

Additional supporting information may be found online in the Supporting Information section at the end of this article.

How to cite this article: Sadekov A, Lloyd NS, Misra S, D'Olivo JP, McCulloch M. *In situ* Mg isotope measurements of biogenic carbonates using laser ablation multi-collector inductively coupled plasma mass spectrometry: A new tool to understand biomineralisation. *Rapid Commun Mass Spectrom*. 2020;34:e8918. <https://doi.org/10.1002/rcm.8918>